bioRxiv preprint doi: https://doi.org/10.1101/391201; this version posted August 14, 2018. The copyright holder for this preprint (which was not certified by peer review) is the author/funder, who has granted bioRxiv a license to display the preprint in perpetuity. It is made available under aCC-BY-NC-ND 4.0 International license.

Deforming the metric of cognitive maps distorts memory

Jacob L.S. Bellmund[1,2,3*], Tom A. Ruiter[1,4], Matthias Nau[1], Caswell Barry[5], Christian F. Doeller[1,2,3,6*]

1: Kavli Institute for Systems Neuroscience, Centre for Neural Computation, The Egil and Pauline Braathen and Fred Kavli Centre for Cortical Microcircuits, NTNU, Norwegian University of Science and Technology, Trondheim, Norway

2: Donders Institute for Brain, Cognition and Behaviour, Radboud University, Nijmegen, the Netherlands

3: Max Planck Institute for Human Cognitive and Brain Sciences, Leipzig, Germany

4: Amsterdam Brain and Cognition, University of Amsterdam, The Netherlands

5: Research Department of Cell and Developmental Biology, University College London, United Kingdom

6: St. Olavs Hospital, Trondheim University Hospital, Trondheim, Norway

* Corresponding authors. Email: jacob.bellmund@ntnu.no; christian.doeller@ntnu.no

Abstract

Entorhinal grid cells, characterized by spatially periodic activity patterns, are thought to provide a universal spatial metric. However, grid cell firing-patterns are distorted in highly polarized environments such as trapezoids. Additionally, the functional role of grid cells in guiding behavior remains elusive. Here, we leverage immersive virtual reality using a novel motion platform to test the impact of environmental geometry on spatial memory in participants navigating a trapezoid arena. Object position memory in the trapezoid was degraded compared to a square control environment. Consistent with grid pattern distortions in rodents, this effect was more pronounced in the narrow than the broad part of the trapezoid. Remarkably, even outside of the encoding environment, these distortions persistently affected both navigated and judged distance estimates of never experienced paths between remembered positions and reconstructed memory maps. These distorted memory maps in turn explained behavior better than objective maps. Our findings demonstrate that environmental geometry interacts with human spatial memory similarly to how it affects rodent grid cells – thus strengthening the putative link between grid cells and behavior as well as cognitive functions beyond navigation.

bioRxiv preprint doi: https://doi.org/10.1101/391201; this version posted August 14, 2018. The copyright holder for this preprint (which was not certified by peer review) is the author/funder, who has granted bioRxiv a license to display the preprint in perpetuity. It is made available under aCC-BY-NC-ND 4.0 International license.

Introduction

The neural basis of navigation and spatial memory is well-studied and has resulted in the identification of functionally defined cell types encoding spatial information relevant to wayfinding (Moser et al., 2017; Epstein et al., 2017). Among these are grid cells, first identified in the entorhinal cortex of freely moving rodents, which exhibit six-fold periodic (hexadirectional) spatial firing extending across the environment (Hafting et al., 2005). This pattern can be described in terms of its scale, as well as its offset and orientation relative to the environment (Hafting et al., 2005; Moser et al., 2017). Along the dorso-ventral axis of medial entorhinal cortex , grid cells sharing similar spacing and orientations are organized in discrete modules (Barry et al., 2007; Brun et al., 2008; Stensola et al., 2012). Grid cells have been directly recorded in human patients undergoing pre-surgical screening (Jacobs et al., 2013; Nadasdy et al., 2017) and in human fMRI studies hexadirectional signals serve as a proxy measure for activity of the entorhinal grid system (Doeller et al., 2010; Kunz et al., 2015; Bellmund et al., 2016; Constantinescu et al., 2016; Horner et al., 2016; Navarro Schröder et al., 2017; Nau et al., 2018; Julian et al., 2018; Stangl et al., 2018).

Theoretical work suggests that regular grid patterns provide a compact code for self-localization and function as a metric for space, supporting path integration and vector-based navigation (Moser et al., 2017; Hafting et al., 2005; McNaughton et al., 2006; Fiete et al., 2008; Burak and Fiete, 2009; Mathis et al., 2012; Bush et al., 2015; Herz et al., 2017; Banino et al., 2018). Thus, location is encoded by the conjunction of spatial phases across different modules – the population phase (Bush et al., 2015; Carpenter and Barry, 2016) – while the distance and direction between points can be derived from the relative difference in population phase (Bush et al., 2015). Yet direct empirical evidence demonstrating the behavioral relevance of grid cells remains scarce. However, in line with the proposed role of grid cells in spatial navigation and memory, the strength and coherence of hexadirectional signals across voxels in human entorhinal cortex predict the accuracy of subjects' spatial memory responses in virtual reality (VR) navigation tasks (Doeller et al., 2010; Kunz et al., 2015).

Despite their regular firing patterns (Hafting et al., 2005) and the consistent behavior of grid cell ensembles across different environments (Fyhn et al., 2007; Yoon et al., 2013) and behavioral states (Gardner et al., 2017; Trettel et al., 2017), environmental geometry strongly influences grid firing patterns (Krupic et al., 2015; Stensola et al., 2015; Sun et al., 2015; Krupic et al., 2018). Thus, changes made to the geometry of a familiar enclosure produce commensurate changes to the scale of grid-patterns, resulting in differential rates of change in population phase for travel in the changed and unchanged dimension (Barry et al., 2007; Stensola et al., 2012). Similar manipulations made while humans navigate in VR environments produce complementary deficits in path integration (Chen et al., 2015). Equally, the configuration of static environments also influences grid regularity, for example, in square

bioRxiv preprint doi: https://doi.org/10.1101/391201; this version posted August 14, 2018. The copyright holder for this preprint (which was not certified by peer review) is the author/funder, who has granted bioRxiv a license to display the preprint in perpetuity. It is made available under aCC-BY-NC-ND 4.0 International license.

enclosures grid firing tends to orient relative to enclosure walls (Krupic et al., 2015; Stensola et al., 2015; Sun et al., 2015). More strikingly, in highly polarized enclosures such as trapezoids, grid-patterns are highly distorted and less regular than in control enclosures (Krupic et al., 2015). These changes were found to be especially pronounced in the narrow part of the trapezoidal enclosure with reduced symmetry, larger firing fields, increased spacing and a change of grid orientation – changes which do not appear to attenuate with continued exposure (Krupic et al., 2015). Similarly, in a quadrilateral environment with one slanted wall, firing fields of grid cells were observed to be consistently shifted away from the slanted wall, resulting in a local distortion of the grid (Krupic et al., 2018). Decoding of positions from simulated grid cells capturing this distortion was less accurate near the slanted wall (Krupic et al., 2018). However, the behavioral consequences of degraded positional information due to a compromised grid pattern, which might result in uncertainties about locations and distances in space (Carpenter and Barry, 2016; Krupic et al., 2015, 2018) (Figure 1), have not been explored. Here, we use environmental manipulations to shed light on how grid cell-based computations might support behavior.

Inspired by the distortions of grid-cell firing patterns in a trapezoidal enclosure in rodents, we investigated the effects of environmental geometry on human spatial memory. We hypothesized that environmental geometry-dependent distortions of the spatial metric provided by grid cell firing would affect mnemonic performance. Specifically, we predicted positional memory to be impaired in a trapezoidal compared to a square control environment. Relatedly, we expected that within the trapezoid performance should be more degraded in the narrow than the broad part of the enclosure. Importantly, object locations encoded using a distorted metric should further persistently affect subsequent spatial computations performed on the distorted memories. We therefore tested whether mnemonic distortions would persist outside of the trapezoidal environment and predicted differential estimates of identical distances between positions located in the narrow and broad part of the trapezoid, respectively.

Results

Positional memory

We employed immersive VR to investigate effects of environmental geometry on human spatial memory (Figure 1). Wearing a head-mounted display, participants navigated a trapezoid and a square environment of equal surface area using a motion platform translating real-world rotations and steps into virtual movement. In both environments, participants learned the positions of six objects, organized in two triplets with matched inter-object distances in both halves of an environment (Figure 1B). Participants were tested on the positions of the objects after an initial learning phase by having to navigate to the

bioRxiv preprint doi: https://doi.org/10.1101/391201; this version posted August 14, 2018. The copyright holder for this preprint (which was not certified by peer review) is the author/funder, who has granted bioRxiv a license to display the preprint in perpetuity. It is made available under aCC-BY-NC-ND 4.0 International license.

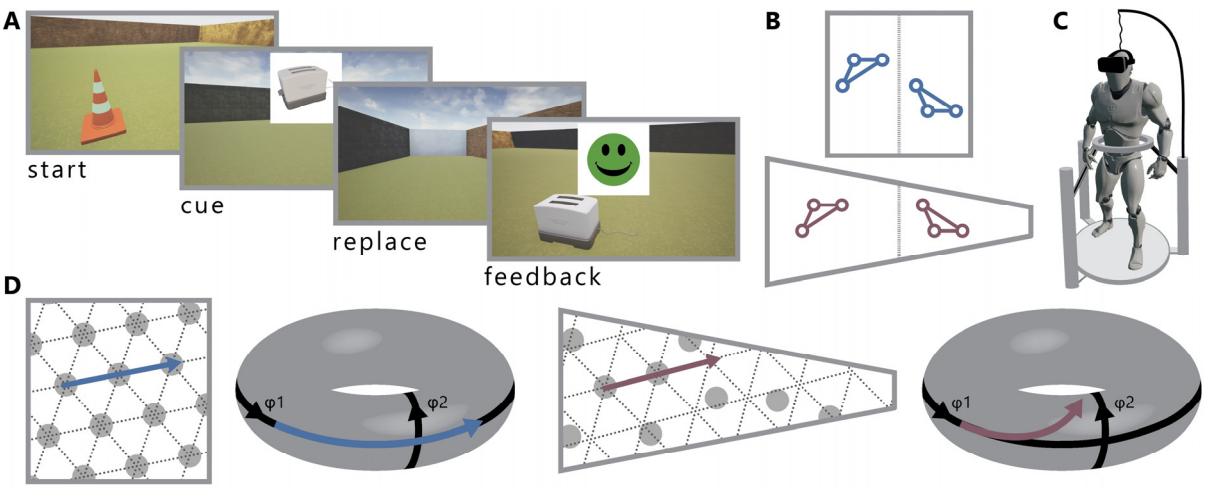

Figure 1. Task design and rationale. A. To commence a trial, participants walked to a start position marked by a pylon where they were cued with the image of an object. Subsequently, they navigated to the object's remembered position, which they indicated via button press, and received feedback. **B**. Circles illustrate an exemplary configuration of object positions. Two triplets of objects were positioned in each environment with one triplet in each half of each environment, yielding four triplets with matched distances between positions. **C**. Schematic of immersive VR setup with head mounted display and motion platform translating physical steps and rotations into virtual movement. **D**. Illustration of regular and distorted grid in square and trapezoidal environment, respectively. Dashed lines indicate axes of idealized grid and grey circles mark corresponding firing fields. The torus provides a continuous representation of the 2D-periodic population phase. Translational movement of a given distance in the square (blue arrow) results in a corresponding change of grid population phase (blue arrow on the torus). In the trapezoidal environment, a movement of the same Euclidean distance (purple arrow) results in a different change in population phase (purple arrow on the torus) due to the degraded grid pattern characterized by reduced symmetry as a result of changes in grid period and orientation. A similar effect is expected between the narrow compared to the broad part of the trapezoid (not shown) due to the more severe distortion of the grid pattern (see Methods).

remembered position of a cued object in each trial (Figure 1A). In a first step, we then compared positional memory, i.e. the Euclidean distance between this response position and the correct position, between the two environments. In line with degradations in grid cell firing patterns observed in rodents (Krupic et al., 2015), results showed larger response errors in the trapezoid than the square (Figure 2A, $t(36)=2.71$, $p=9.999\times10^{-5}$; bootstrap-based t-tests are reported throughout the manuscript, see Methods).

To ensure that this effect was not due to the fact that larger error distances are possible within the trapezoid because of its elongated shape, we calculated memory scores to account for differences in the distribution of possible errors for each position (Jacobs et al., 2016). In short, we generated a set of 1000 random locations uniformly covering the entire environment, compared the error distance of a given trial to the distances from the random locations to the trial's correct position and quantified the memory score as the proportion of random locations further away from the correct position than the observed response position. This yielded a score ranging from 0 (low memory) to 1 (perfect memory) for each

bioRxiv preprint doi: https://doi.org/10.1101/391201; this version posted August 14, 2018. The copyright holder for this preprint (which was not certified by peer review) is the author/funder, who has granted bioRxiv a license to display the preprint in perpetuity. It is made available under aCC-BY-NC-ND 4.0 International license.

trial, taking into account the range of possible errors based on the correct position and environmental geometry (Figure 2B). Importantly, memory scores were significantly lower in the trapezoid compared to the square (Figure 2C, $t(36)=-2.30$, $p=5.000\times10^{-4}$), ensuring that decreased positional memory was not due to different distributions of possible errors as a result of the elongated shape of the trapezoid.

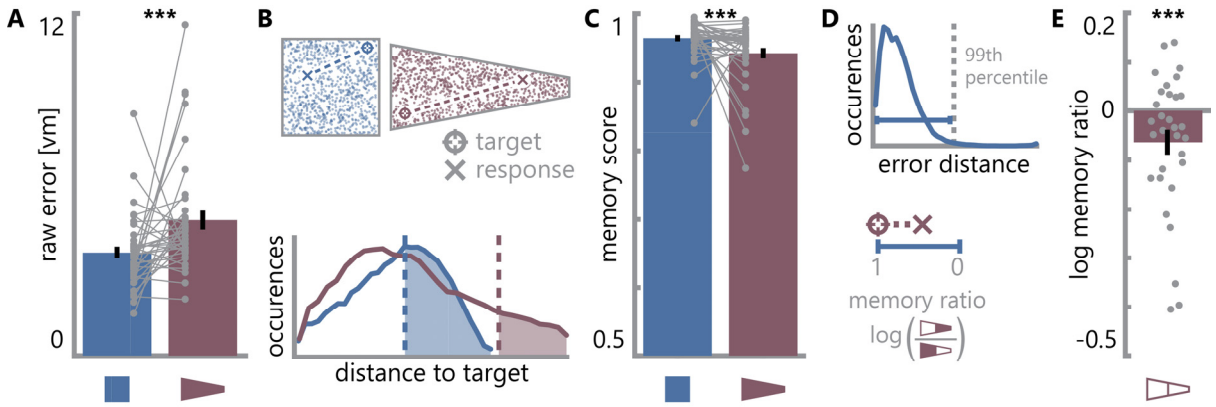

Figure 2. Distorted positional memory in the trapezoid. A. Raw replacement errors in virtual meters (vm) as measured by the distance between the correct and remembered position were larger for object positions in the trapezoid than in the square. **B**. Schematics illustrate the expression of positional memory using memory scores for two hypothetical trials. For both environments a distribution of random positions uniformly covering the available space was generated (top). For each trial, mnemonic performance was expressed as a memory score quantifying the proportion of random positions further away from the correct object position than the response location (bottom). **C**. Memory scores were lower in the trapezoid than in the square environment. Y-axis thresholded at chance level of 0.5. **D**. Schematics illustrate calculation of the memory ratio. Using the 99th percentile of error values across all participants and trials in the square environment as a reference (top), we quantified performance in the narrow and broad part of the trapezoid on a scale from 1 (perfect memory) to 0 (replacement error the same size or larger than the reference value obtained from performance in the square). The log memory ratio contrasts average performance in the narrow and broad part of the trapezoid. **E**. The memory ratio was significantly below 0, indicating lower positional memory in the narrow compared to the broad part of the trapezoid. 6 participants were excluded due to log memory ratios more than 1.5 times the interquartile range above or below the upper and lower quartile respectively. See Supplemental Figure 1B for full dataset. All bars show mean±SEM, grey circles indicate individual subject data with lines connecting data points from the same participant. *** $p<0.001$

In rodents, entorhinal grid-patterns are most distorted in the narrow part of the trapezoid enclosure (Krupic et al., 2015). Building on this observation, we predicted that positional memory should follow this pattern if such deformations are indeed detrimental to spatial memory. To account for the overall high performance levels of participants (Supplemental Figure 1A), we referenced memory performance in the trapezoid to memory performance in the square to allow for a comparison of replacement errors between the two parts of the environment despite differences in local geometry. Specifically, we chose the 99th percentile

bioRxiv preprint doi: https://doi.org/10.1101/391201; this version posted August 14, 2018. The copyright holder for this preprint (which was not certified by peer review) is the author/funder, who has granted bioRxiv a license to display the preprint in perpetuity. It is made available under aCC-BY-NC-ND 4.0 International license.

of error distances across all trials and participants as a reference. Each trial was then assigned a score calculated as one minus the proportion of its replacement error of this reference value obtained from the square (Figure 2D). This resulted in memory scores, comparable across subjects, with larger values indicating better performance. To compare positional memory between the narrow and broad part of the trapezoid we calculated the log memory ratio to quantify the relation of mean memory scores in the two parts. This ratio was significantly below 0 (Figure 2E, $t(30)=-2.52$, $p=9.999\times10^{-5}$), indicating decreased memory performance in the narrow compared to the broad part of the environment. This was also true for the memory ratio calculated from the raw error scores (Supplemental Figure 1B). The log memory ratio of the trapezoid was lower than the 5th percentile of a surrogate distribution of memory ratios obtained from comparing positional memory between the halves of the square, indicating a significant difference between the environments (Supplemental Figure 1C, $Z=-2.48$, $p=0.007$). Taken together, the profile of positional memory observed is in line with our predictions derived from deformations of grid cell firing patterns with degraded positional memory in the trapezoidal compared to the square environment and more impaired performance in the narrow than the broad part of the trapezoid.

These differences in positional memory were not due to differential navigation behavior: The excess path length of participants' navigation paths from the start position of a given trial to where they remembered the object did not differ in the trapezoid compared to the square environment or between the two parts of the trapezoid (Supplemental Figure 2, square vs. trapezoid: $t(36)=-0.95$, $p=0.144$; broad vs. narrow trapezoid: $t(36)=-0.11$, $p=0.865$). Further, walking speeds did not differ between the two environments or the sub-parts of the trapezoid (Supplemental Figure 2, trapezoid vs. square: $t(36)=-0.01$, $p=0.973$; broad vs. narrow trapezoid: $t(36)=1.15$, $p=0.079$). Euclidean distances from the start to the correct object positions were not related to spatial memory performance (Supplemental Figure 2, square: $t(36)=0.17$, $p=0.863$, trapezoid: $t(36)=0.17$, $p=0.869$, trapezoid broad: $t(36)=1.37$, $p=0.177$, trapezoid narrow: $t(36)=-0.01$, $p=0.998$).

To explore participants' navigation behavior in more detail we next examined their body and head orientation during the replacement period relative to the direction from start to response position in each trial (Supplemental Figure 3). Both body and head orientation of participants were significantly clustered around this direction in square (body: $v=36.84$, $p=1.086\times10^{-17}$; head: $v=36.68$, $p=1.500\times10^{-17}$) and trapezoid (body: $v=36.89$, $p=9.738\times10^{-18}$; head: $v=36.68$, $p=1.490\times10^{-17}$) and the distributions of mean orientations were not different between the two environments (body: $F(1,72)=0.02$, $p=0.889$; head: $F(1,72)=0.14$, $p=0.709$). Similar results were obtained for the body and head orientations when comparing trials targeting objects in the broad and narrow parts of the trapezoid (body broad: $v=36.73$, $p=1.357\times10^{-17}$; body narrow: $v=36.73$, $p=1.350\times10^{-17}$; difference body: $F(1,72)=1.53$, $p=0.220$; head broad: $v=36.54$, $p=1.957\times10^{-17}$; head narrow: $v=36.65$, $p=1.579\times10^{-17}$; difference head

bioRxiv preprint doi: https://doi.org/10.1101/391201; this version posted August 14, 2018. The copyright holder for this preprint (which was not certified by peer review) is the author/funder, who has granted bioRxiv a license to display the preprint in perpetuity. It is made available under aCC-BY-NC-ND 4.0 International license.

F(1,72)=0.05, p=0.830). Hence, we do not expect average facing direction to influence our key comparisons between the two environments or within the trapezoid. The circular variance around each trial's average body direction did not differ between environments (trapezoid vs. square: t(36)=1.06, p=0.118) or the trapezoid parts (narrow vs. broad: t(36)=1.14, p=0.076), but the circular variance of participants' facing directions was greater in the trapezoid than in the square (t(36)=2.57, $p=9.999\times10^{-5}$) and greater in the narrow than broad part of the trapezoid (t(36)=2.13, $p=5.000\times10^{-4}$), potentially reflecting increased visual exploration and orientation to compensate for impaired spatial memory. Do attentional resources and task demands differ between test environments? This seems unlikely as our design included a secondary task in which participants memorized color changes of an extramaze cue and later estimated durations between color change events (see Methods). Mean (t(36)=-0.10, p=0.873) and absolute (t(36)=-0.32, p=0.629) estimation errors as well as error variability (t(36)=-0.81, p=0.205) did not differ between square and trapezoid (Supplemental Figure 6), suggesting comparable attentional resources were available in both environments.

Mnemonic distortions outside of the environment

Next, we sought to address whether the impact of environmental geometry on spatial memory persisted outside of the learning environment. To this end, we asked participants to estimate distances between the positions of object pairs in two modalities subsequent to the encoding phase in VR. In the VR version of the distance estimation task, participants reported distances by walking the respective distance between two remembered object positions in a circular enclosure. In the desktop version of this task, they indicated these distances on a subjective scale (Figure 3, see Methods). Participants successfully completed both versions of the task (Supplemental Figure 4AB; long vs short distances in VR version: t(36)=11.00, $p=9.999\times10^{-5}$; mean±SD of Spearman correlations between true and estimated distances in desktop version: r=0.67±0.19), demonstrating the ability to compute never-experienced distances from pairs of remembered positions. Comparing distances walked in the VR version of the task to true Euclidean distances across all trials revealed an overestimation bias (t(36)=5.78, $p=9.999\times10^{-5}$).

The regular firing patterns of grid cells are assumed to support vector calculations, allowing navigational vectors to be calculated by comparing the current grid population phase with the phase of remembered locations (Banino et al., 2018; Bush et al., 2015; Erdem and Hasselmo, 2012; Fiete et al., 2008; Kubie and Fenton, 2012). Therefore, the differences in grid cell firing patterns between the narrow and the broad part of the trapezoid (Krupic et al., 2015) might result in differential estimates for distances of the same magnitude. More specifically, differences in the change of grid population phase between equidistant positions might explain such an effect (Carpenter and Barry, 2016) (Figure 1D). Taking advantage of our design in which participants learned a triplet of object positions in each half of an environment with matched inter-object distances, we tested this hypothesis by

bioRxiv preprint doi: https://doi.org/10.1101/391201; this version posted August 14, 2018. The copyright holder for this preprint (which was not certified by peer review) is the author/funder, who has granted bioRxiv a license to display the preprint in perpetuity. It is made available under aCC-BY-NC-ND 4.0 International license.

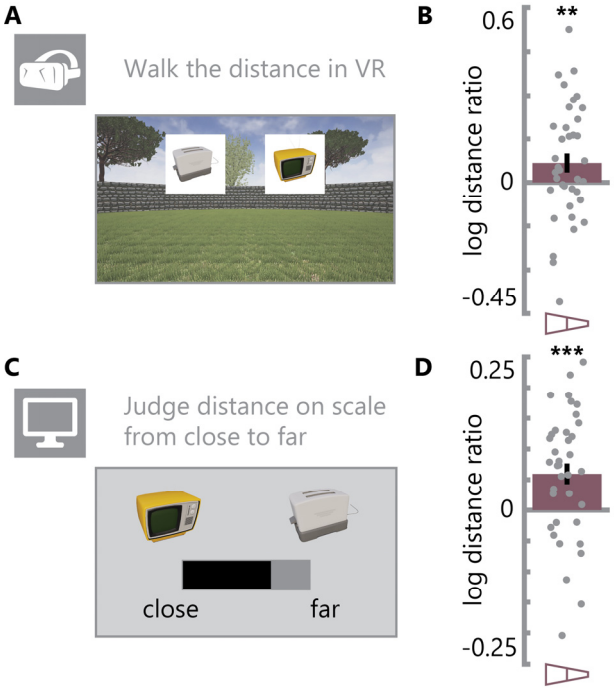

Figure 3. Distortion of distance estimates. A. Participants were cued to estimate and walk distances between the remembered positions of object pairs in a circular virtual environment. **B.** Taking advantage of matched distances between object positions, estimated distances were averaged for each triplet and expressed as a distance ratio of estimated distances in the narrow over the broad part of the trapezoid. The log distance ratio differed significantly from 0. **C.** In the desktop version of the task, participants adjusted a slider to estimate the distance between object pairs on a subjective scale from close together to far apart. **D.** The estimates for the same distances differed between the two parts of the trapezoid as indicated by the log distance ratio, which was significantly different from 0. All bars show mean±SEM and grey circles indicate individual subject data. ** $p<0.01$, *** $p<0.001$

comparing the distances remembered for the two triplets. The log ratio of mean remembered distances between the narrow and broad part of the trapezoid was significantly different from 0 in both the VR (Figure 3B, $t(36)=2.04$, $p=0.001$) and the desktop (Figure 3D, $t(36)=3.49$, $p=9.999\times10^{-5}$) version of the task, indicating that participants consistently estimated the same distances in the two parts of the trapezoid as different. Indeed, the ratio of remembered distances was highly correlated across the two modalities (Supplemental Figure 4C, Spearman $r=0.71$, $p=1.984\times10^{-6}$). In both versions of the task, the distance ratio of the trapezoid differed significantly from the surrogate distributions of distance ratios obtained from the square (Supplemental Figure 4DE, VR: $Z=3.27$, $p=0.001$; desktop: $Z=4.09$, $p=2.138\times10^{-5}$).

Reconstruction of remembered locations

What is the structure of deformed memory maps? To reconstruct remembered object positions from estimated inter-object distances, we applied multidimensional scaling to the data obtained in the desktop version of the task (Figure 4A). We extracted coordinates along two dimensions (see Supplemental Figure 5A) which we mapped onto the true coordinates of the trapezoid using Procrustes analysis to match the two configurations of coordinates (Figure 4A and Supplemental Figure 5B, see Methods). We quantified the deviance between the true and reconstructed positions after Procrustes analysis and compared this Procrustes distance to a surrogate distribution of distances obtained from shuffling object-position-assignments to assess the statistical significance of the reconstruction accuracy (Figure 4B). The observed Procrustes distances were significantly lower than the 5th percentiles of the surrogate distributions (Figure 4C, $t(36)=-8.48$, $p=9.999\times10^{-5}$), reflecting a close match between true and reconstructed positions. Importantly, re-calculating above-described

bioRxiv preprint doi: https://doi.org/10.1101/391201; this version posted August 14, 2018. The copyright holder for this preprint (which was not certified by peer review) is the author/funder, who has granted bioRxiv a license to display the preprint in perpetuity. It is made available under aCC-BY-NC-ND 4.0 International license.

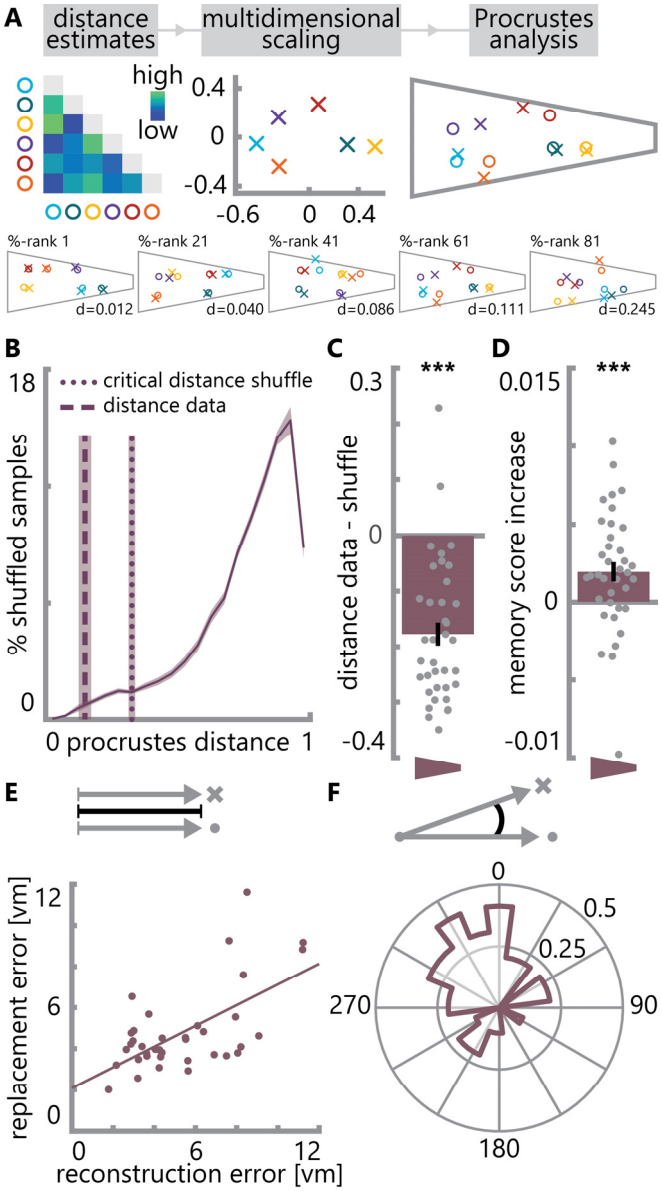

Figure 4. Reconstruction of remembered positions. A. Using multidimensional scaling (MDS), coordinates along two underlying dimensions were extracted from pairwise distance estimates. The resulting coordinates were mapped to the original object positions in the trapezoid using Procrustes analysis (see Methods). Color bar indicates estimated distances. Data shown for a randomly selected participant in top panel. Bottom row shows five participants chosen to illustrate reconstruction accuracy across the sample based on the spread of Procrustes distances (data shown for participants at percent ranks 1, 21, 41, 61 and 81 from left to right). Colored circles indicate correct positions and crosses the respective reconstructed positions. **B.** The Procrustes distance quantifies the deviation between true and reconstructed positions as the normalized sum of squared error distances (mean across participants shown by dashed vertical line). For each participant, a surrogate distribution of Procrustes distances was obtained from fitting the coordinates from MDS to coordinate sets with shuffled object identities (solid line). Dotted vertical line indicates the averaged critical Procrustes distance defined as the 5th percentile of the respective surrogate distributions. Shaded areas show SEM across participants. **C.** The Procrustes distances from fitting to true coordinates were significantly smaller than the critical distances of the surrogate distributions. **D.** Memory scores quantifying positional memory within the environment were significantly higher when calculated with respect to the reconstructed rather than the true object positions. **E.** The average lengths of vectors from true object positions to response and reconstructed positions correlate across participants **F.** The angular difference in orientation between vectors from true object positions to response and reconstructed positions clusters around zero. Bars in **C** and **D** show mean±SEM and grey circles indicate individual subject data. *** $p<0.001$

memory scores with the reconstructed positions led to higher scores compared to the true positions (Figure 4D, $t(36)=3.09$, $p=9.999\times10^{-5}$), providing direct evidence that positional

bioRxiv preprint doi: https://doi.org/10.1101/391201; this version posted August 14, 2018. The copyright holder for this preprint (which was not certified by peer review) is the author/funder, who has granted bioRxiv a license to display the preprint in perpetuity. It is made available under aCC-BY-NC-ND 4.0 International license.

memory is used to compute distances between objects and that distorting the spatial map also distorts distance estimates. This effect was also significant when excluding trials targeting objects whose reconstructed position lay outside of the environment ($t(36)=1.42$, $p=0.023$). For each participant, we then calculated the error vectors between the true and remembered positions in the object position memory task and compared these to the error vectors of the reconstructed positions. Overall, there was a strong relationship between reconstructed and remembered positions as indicated by a significant correlation of the average lengths of the error vectors (Figure 4E, $r=0.62$, $p=4.917\times10^{-5}$) and a clustering of their directions (Figure 4F, angular difference of vectors significantly clustered around 0: $v=13.77$, $p=0.001$).

Discussion

Here, we used immersive VR to demonstrate that environmental geometry can distort human spatial memory. Consistent with environmentally-induced distortions of rodent entorhinal grid-patterns, our data show that positional memory is impaired in a trapezoid compared to a square with the deficits being most pronounced in the narrow end of the trapezoid environment. Importantly, the distortions persisted outside of the environment as participants estimated identical distances to be different between the narrow and broad part of the trapezoid, underscoring the effect of environmental geometry during encoding on subsequent memory. Moreover, remembered positions reconstructed from these distance estimates directly reflected positional memory during the learning task.

Our findings indicate a strong influence of environmental geometry on human spatial memory. This influence has been predicted from rodent data in which the six-fold symmetry of grid firing is distorted in a trapezoidal enclosure, with the most pronounced distortions in the narrow part of the enclosure (Krupic et al., 2015). These irregularities are manifest as changes in the scale and orientation of firing patterns (Krupic et al., 2015). The grid cell population phase is thought to provide a mechanism to encode spatial positions and calculate vectors between locations (Bush et al., 2015). As such, distortions of the grid-pattern will decouple the rate of change in population phase from distance traveled (Carpenter and Barry, 2016). Concurrent with impaired positional decoding from simulated grid cells with locally distorted firing patterns (Krupic et al., 2018), this might lead to uncertainty in the discrimination of positions in space and ultimately result in impaired positional memory and diverging distance estimates for the same Euclidean distances. In concert with evidence for impaired path integration with disrupted grid cell firing in rodents (Gil et al., 2018) and increased path integration errors in older adults with weaker hexadirectional signals measured with fMRI (Stangl et al., 2018), previous studies support the interpretation that the integrity of the grid pattern is beneficial for human spatial memory. The strength of hexadirectional signals and the directional coherence of the orientation of these signals across voxels in the entorhinal cortex are associated with memory performance

bioRxiv preprint doi: https://doi.org/10.1101/391201; this version posted August 14, 2018. The copyright holder for this preprint (which was not certified by peer review) is the author/funder, who has granted bioRxiv a license to display the preprint in perpetuity. It is made available under aCC-BY-NC-ND 4.0 International license.

across participants learning object positions in circular enclosures (Doeller et al., 2010; Kunz et al., 2015). Our findings dovetail with this notion as they demonstrate that environmental geometry, known to compromise grid-patterns in rodents, influences spatial cognition in a within-subject design.

Prior studies suggested that changing environmental boundaries might influence human spatial cognition in ways consistent with findings from studies of rodent place (O'Keefe and Dostrovsky, 1971) and grid cells (Hafting et al., 2005). Focusing on path integration, one of the core functions assumed for grid cells (Hafting et al., 2005; McNaughton et al., 2006; Moser et al., 2017), biases in human navigation have been reported to follow predictions derived from grid cell firing (Chen et al., 2015). In particular, the experimental design in Chen et al. (2015) built upon the observation that rodent grid-patterns rescale to match changes made to the geometry of already familiar enclosures (Barry et al., 2007). Expansions and compressions of boundaries relative to preceding trials resulted in under- and overshoots of the return path in a path integration task, when the path included a component along the manipulated boundary dimension (Chen et al., 2015). This illustrates how, through environmental change, altering the rate of change in grid cell population phase in relation to distance traveled can introduce biases in human navigation (Carpenter and Barry, 2016; Chen et al., 2015). Translating this idea to the memory-based estimation of distances between locations might explain the diverging judgments of identical distances observed in our data. Expansions and compressions of virtual environments have further been demonstrated to impact spatial memory in humans and under conditions of environmental change, positional memory follows models of place cells and boundary proximity (Hartley et al., 2004; Schuck et al., 2015). While the studies described above indicate how boundary manipulations in familiar environments influence spatial behavior, we built upon work showing that distorted grid-patterns persist in static trapezoid environments even with prolonged experience (Krupic et al., 2015). Our findings suggest that distortions of the brain's spatial metric can result in mnemonic distortions under constant boundary conditions within a specific environment and even outside of this encoding environment.

We opted for a purely behavioral experiment; our hypotheses, experimental design and analysis however directly built upon findings from electrophysiological recordings of grid cells in rodents (Krupic et al., 2015). We employed highly immersive VR technology to enhance the impact of environmental geometry on spatial cognition and engage proprioceptive, vestibular and motor systems during the task. Currently, immersive VR does not allow the concurrent recording of neural data. The contribution of locomotor cues to the experience of navigation in general has been emphasized previously (Taube et al., 2013) and a recent study in rodents has used gain manipulations in VR to emphasize the contributions of locomotor cues to grid cell firing specifically (Campbell et al., 2018). Having established the impact of environmental geometry on human spatial cognition, an exciting question for future research would be to combine manipulations of environmental geometry with

bioRxiv preprint doi: https://doi.org/10.1101/391201; this version posted August 14, 2018. The copyright holder for this preprint (which was not certified by peer review) is the author/funder, who has granted bioRxiv a license to display the preprint in perpetuity. It is made available under aCC-BY-NC-ND 4.0 International license.

neuroimaging techniques such as fMRI to study the deformations of the cognitive map we describe here in the brain. To do so, an important measure could be the hexadirectional signal that can be observed in the human entorhinal cortex (Doeller et al. 2010). Beyond fMRI, an exciting future avenue is paved by the development of new magnetoencephalography systems, which might allow the combination of immersive VR with recordings of neural data (Boto et al., 2018).

As large parts of human indoor navigation take place in rectangular rooms, the novelty of a trapezoidal enclosure in our task might be considered as a factor contributing to impaired performance compared to the square. Such an effect of unfamiliarity with polarized environments, however, would not predict the observed within-environment differences in performance. Further, participants' walking speeds did not differ between environments and their paths from the start to the remembered object position were not more or less direct. Thus, none of our control measures provided evidence for fundamental differences in navigational performance between the environments per se. The absence of differences in navigation performance is in line with the successful use of trapezoidal room geometry during spatial updating (Kelly et al., 2008). Additionally, the detection and encoding of color change events was not affected by the environmental manipulation, speaking against an effect of increased task demand in the trapezoid as sufficient attentional resources were available for this secondary task.

Importantly, the effects we observed in positional memory persisted outside of the environment as demonstrated by the differential estimates for matched distances between positions within the different parts of the trapezoid. These distortions were consistent across response modalities. The response profiles observed in the VR version of the task revealed a general tendency to overestimate distances between positions, in line with previous studies reporting overestimations of navigated distances (Brunec et al., 2017) and spatial scale in map drawings (Jafarpour and Spiers, 2017). We used the distances estimated on a subjective scale in the desktop version of the task to reconstruct remembered positions. Accounting for the distortions in participants' memory by using these reconstructed positions to re-compute memory scores yielded increased performance scores. This illustrates the close match between positions reconstructed from distance estimates and positional memory within the environment, and demonstrates that, consistent with the formation of cognitive maps (O'Keefe and Nadel, 1978), distances never directly experienced in the task were computed from remembered positions. Grid cells have been suggested to support this kind of vector computation (Bush et al., 2015; Banino et al., 2018). This is further in line with evidence for the involvement of the entorhinal grid system in imagination (Bellmund et al., 2016; Horner et al., 2016) and theoretical accounts proposing a role for spatially tuned cells in memory (Byrne et al., 2007; Buckner, 2010; Hasselmo, 2011).

bioRxiv preprint doi: https://doi.org/10.1101/391201; this version posted August 14, 2018. The copyright holder for this preprint (which was not certified by peer review) is the author/funder, who has granted bioRxiv a license to display the preprint in perpetuity. It is made available under aCC-BY-NC-ND 4.0 International license.

The persistent effects of environmental geometry outside of the highly polarized environment also speak to a growing body of literature implicating grid cells in mapping continuous, task-relevant dimensions beyond navigable space. Grid cells have been implicated in mapping visual space in monkeys (Killian et al., 2012) and humans (Nau et al., 2018; Julian et al., 2018) as well as time during running in place throughout a delay (Kraus et al., 2015) and tone frequency during sound sweeps towards a target frequency (Aronov et al., 2017) in rodents. In humans, hexadirectional signals were also observed during trajectories through an abstract space spanned by the dimensions of neck and leg length of stick figure birds (Constantinescu et al., 2016). Collectively, these findings point towards a role of the entorhinal grid system in representing dimensions of task feature spaces. As proposed for navigable space (Hafting et al., 2005; McNaughton et al., 2006; Bush et al., 2015; Moser et al., 2017; Herz et al., 2017), the regular firing patterns of grid cells might provide a metric for these spaces allowing the efficient encoding of specific stimuli located at different positions within a space. Speculatively, correlated feature dimensions or feature spaces in which subsets of feature combinations are impossible might distort how grid cells map these spaces in a similar way as environmental geometry distorts grid cell firing patterns, resulting in biased representations similar to the distortions of spatial memory observed in this study.

In conclusion, our data show distortions of human spatial memory consistent with the changes induced in rodent grid cell activity by the geometry of highly polarized enclosures. These distortions persist outside of the environment, indicating an enduring impact of environmental geometry on memory. In line with the proposed roles for grid cells in navigation and mapping feature dimensions beyond navigable space, these findings suggest that environmental geometry might be able to distort the metric of cognitive representations.

Methods

Participants

53 Participants between the age of 18 and 30 were recruited from the Norwegian University of Science and Technology. All participants provided written informed consent before participation, and all research procedures were approved by the regional ethics committee (REC North, reference number 2017/153). Sample size was based on a power calculation assuming a small to medium effect (d=0.4) of environmental geometry on human spatial cognition, resulting in a sample size of 52 to achieve a statistical power of 80% ($\propto$=0.05, two-tailed test). 39 participants (mean age 23.8±2.5 years, 36% female) completed the experiment (14 incomplete datasets due to technical difficulties with the VR setup or motion sickness). Two participants were excluded due to poor memory performance defined as average replacement errors more than 1.5 times the interquartile range larger than the upper quartile of average errors in the sample. Thus, 37 participants entered the analyses.

bioRxiv preprint doi: https://doi.org/10.1101/391201; this version posted August 14, 2018. The copyright holder for this preprint (which was not certified by peer review) is the author/funder, who has granted bioRxiv a license to display the preprint in perpetuity. It is made available under aCC-BY-NC-ND 4.0 International license.

Overview

Over the course of the experiment, participants completed the object position memory task in two environments and estimated durations between (color change) events occurring during these navigation tasks as well as distances between pairs of object positions. The general structure was as follows: Participants were first familiarized with the VR setup and the time estimation task before beginning the object position memory task in the first environment. The object position memory task was carried out in a trapezoidal or square environment for 20 minutes each, with the order of environments counterbalanced across participants. Subsequent to navigating an environment, participants were prompted to estimate the durations between color change events encountered in that environment. In the last two tasks, participants were prompted to estimate distances between pairs of objects in VR and on a computer screen, respectively. The design of each task and the corresponding analyses are described in detail in the following sections. All analyses were performed using Matlab (Release 2017a, The MathWorks, Inc.) and statistical tests (two-tailed unless stated otherwise) were performed using the Resampling Statistical Toolkit (http://www.mathworks.com/matlabcentral/fileexchange/27960-resampling-statistical-toolkit). Specifically, test statistics were compared against a surrogate distribution obtained from 10000 bootstrap samples respecting within-subject dependencies. Circular statistics were implemented using the Matlab-based Circular Statistics Toolbox (Berens, 2009).

Virtual reality

Aiming to maximize the feeling of immersion and thereby the impact of environmental features we employed state of the art VR technology consisting of a head mounted display (HMD, Oculus Rift CV1) and a motion platform (Cyberith Virtualizer). Participants wore low-friction overshoes and were strapped into a harness attached to the motion platform's ring system allowing free rotations. To navigate the virtual environments, participants were instructed to lean slightly into the ring construction to slide the front foot backwards across the sensors of the low-friction base plate of the motion platform while taking a step forward with the back foot (see Supplementary Video 1), generating translational movement in the current forward direction determined by the orientation of the participant in the ring system (Cakmak and Hager, 2014). Head movements were tracked in 3D using the HMD's tracking system and the virtual environments were displayed to both eyes separately at a resolution of 1080 x 1200 pixels and a refresh rate of 90 Hz. The virtual environments were created and presented using the Unreal Engine (v.4.13.2, Epic Games Inc., 2017) and participants' eye height was set to 1.80 virtual meters (vm). Participants were familiarized with the VR setup in a circular environment (45.74vm in diameter) consisting of a grass floor curtailed by a wall (height 3.75vm). A set of trees spread around the outside the environment served as cues for orientation. During familiarization, participants practiced walking and turning by navigating the circular environment to collect coins appearing at random positions in the environment.

bioRxiv preprint doi: https://doi.org/10.1101/391201; this version posted August 14, 2018. The copyright holder for this preprint (which was not certified by peer review) is the author/funder, who has granted bioRxiv a license to display the preprint in perpetuity. It is made available under aCC-BY-NC-ND 4.0 International license.

Participants were instructed to walk towards the coins and collect them via button presses on a handheld controller. Additionally, this familiarization period served as a practice for the time estimation task (see below).

Object position memory task

Participants performed an object position memory task during which they iteratively learned the positions of six objects in a trapezoidal environment (36vm×76vm×8vm×76vm) with side lengths proportional to the enclosure rodents explored in a study reporting distortions of grid cell firing patterns (Krupic et al., 2015). To establish a behavioral baseline, participants performed this task also in a square control environment (40.27vm×40.27vm) with equal surface area. There were no distal cues outside of the environment to enforce spatial learning based on environmental geometry. To facilitate orientation, each wall was presented in a unique color. Both environments had a grass floor and a blue sky with moving clouds was visible (Figure 1A). Participants performed the task for 20 minutes in each environment with the order counterbalanced across participants. In each environment, participants learned the positions of six everyday objects presented as three-dimensional models. The assignment of objects to arenas and positions was randomized across participants.

In each trial of an initial learning phase, participants navigated to a start position indicated by a traffic cone. Then, an object was shown at its predefined position in the environment and participants were instructed to navigate to the object, collect it via button press and memorize its position. Each object was shown once and the order of objects was randomized. In the subsequent test phase (Figure 1A), participants again navigated to start positions. Upon arrival, a picture of one of the objects was shown as a cue for 3 seconds in front of the participant, prompting participants to navigate to where they remembered this object in the environment. Participants indicated the remembered position via button press after arrival and received feedback about their accuracy in the form of one of five smiley faces. The object then appeared at its correct position and participants collected it before the beginning of the next trial. Participants completed 30.54±6.71 and 30.38±8.09 (mean±SD) test trials in square and trapezoid, respectively (number of trials not significantly different: $t(36)=0.18$, $p=0.759$).

The order of trials was randomized for mini-blocks of six trials, so that within a mini-block each object was sampled once and no two consecutive trials sampled the same objects. A triplet of object positions (Figure 1B) was randomly generated for each participant with a minimum distance of 11vm between object positions and a minimum of at least 3vm to the nearest boundary. Positions were constrained so that the connection between two objects was parallel to the long-axis of the trapezoid or one of the walls of the square. The third object was placed at an angle ranging from 90°-120° relative to the first two with the same distance to one of the objects as between the first two. Such a triplet of positions was placed in both the narrow and broad part of the trapezoid defined based on the midpoint of its

bioRxiv preprint doi: https://doi.org/10.1101/391201; this version posted August 14, 2018. The copyright holder for this preprint (which was not certified by peer review) is the author/funder, who has granted bioRxiv a license to display the preprint in perpetuity. It is made available under aCC-BY-NC-ND 4.0 International license.

long-axis and the left and right part of the square. Placing triplets of objects with matched distances in each part of the environment allowed direct comparisons of remembered distances between environments and their sub-parts (see distance estimation tasks). Since cues were only shown once participants arrived at the start position of a given trial, participants never walked the direct path between two objects. Distances from start to target object positions (mean and standard deviation square: 18.66±4.65vm; trapezoid: 19.92±8.50vm; trapezoid broad: 21.10±10.95vm; trapezoid narrow: 18.73±4.67vm) did not influence spatial memory performance (Supplemental Figure 2EF).

Positional memory

Replacement errors were quantified as the Euclidean distance between the correct position of an object in the environment and the position remembered by the participant. To limit the influence of outlier trials we excluded trials with replacement errors larger than 1.5 times the interquartile distance above the upper quartile of errors for each participant (mean±SEM number of trials excluded =3.35±0.26) from all further analyses. Average replacement errors were compared across environments using a bootstrap-based paired t-test (Figure 2B). To account for the fact that despite equal area larger replacement errors are possible in the trapezoid compared to the square control environment, we subsequently quantified performance using memory scores. Specifically, we generated a distribution of 1000 random locations uniformly covering each environment and quantified for each trial the proportion of locations further away from the correct object position than the position indicated by the participant. Importantly, calculating memory scores based on the distribution of possible errors for each target position yields a measure comparable across positions and environments (Jacobs et al., 2016) with a chance level of 0.5 for random performance and scores closer to 1 for high performance. To test the hypothesis of degraded spatial memory in the trapezoid memory scores were compared across environments using a bootstrap-based paired t-test (Figure 2C).

In a next step, we aimed to test the more specific hypothesis of increased degradation of positional memory in the narrow compared to the broad part of the trapezoid derived from the larger distortions of firing patterns of grid cells in this part of the environment (Krupic et al., 2015). To account for the high performance levels of our participants compared to the baseline of chance performance and differences in local geometry, we referenced performance in the trapezoid to performance in the square control environment for this analysis (Figure 2D). Specifically, the 99th percentile of replacement errors across all participants and trials served as a reference value to quantify performance in each single trial as 1 minus the quotient of a trial's error and the reference value, resulting in higher scores for better performance. Trials with errors larger than the reference value were assigned a score of 0, attenuating the effects of trials with very large errors. For each participant, we calculated the ratio of scores averaged across object positions in the narrow and broad part of the trapezoid, respectively. After log transformation, we again used a bootstrap-based t-

bioRxiv preprint doi: https://doi.org/10.1101/391201; this version posted August 14, 2018. The copyright holder for this preprint (which was not certified by peer review) is the author/funder, who has granted bioRxiv a license to display the preprint in perpetuity. It is made available under aCC-BY-NC-ND 4.0 International license.

test to test whether the resulting ratio was significantly below 0 (Figure 2E). Outlier participants were excluded based on our standard criterion of values more than 1.5 times the interquartile range above or below the upper or lower quartile, respectively (see Supplemental Figure 1B for full dataset). The memory ratio also differed significantly from 0 when calculated using raw errors (Supplemental Figure 1B). Note that when calculating the memory ratio based on raw error scores we divided errors in the broad by errors in the narrow part of the trapezoid so that low values of the memory ratio consistently reflected impaired performance in the narrow part of the environment. Since the rotationally symmetric geometry of the square does not pre-define how to calculate the memory ratio, we created a surrogate distribution by shuffling which half of the environment was to serve as the numerator and denominator for the memory ratio across participants. For each permutation, we calculated the ratio between memory performance (expressed relative to the same reference value as for the trapezoid) for objects located in the two halves of the square. The log memory ratio observed in the trapezoid was smaller than the 5th percentile (one-tailed test) of the surrogate distribution obtained from 10000 permutations, (Supplemental Figure 1C). The shape of the surrogate distribution did not differ from normality (Kolmogorov-Smirnov test, D=0.001, p=0.521), we hence used it to convert the p-value reflecting the number of occurrences of smaller memory ratios in the surrogate distribution into a Z-statistic. To visualize response behavior in the two parts of the trapezoid we collapsed across all trials from all participants for objects located in the broad and narrow part of the arena. Response positions were centered on the respective true positions and divided into 50x50 square bins with a side length of 0.6vm. The resulting histogram was smoothed using a Gaussian kernel with a standard deviation of 0.5vm and plotted as a heatmap (Supplemental Figure 1D).

Parameters of navigation

To assess whether differences in navigation behavior might underlie the observed differences in positional memory, we analyzed navigational performance in the replacement phase of each trial, where participants navigated to the remembered position of a cued object. For each trial, we calculated the Euclidean distance between the start position and the response location and subtracted it from the length of the path walked by the participant. This excess path length measures the directness of the paths taken, potentially reflecting the degree of certainty about the trajectory as increased uncertainty might lead to more turns and longer paths. We contrasted averaged excess path lengths between the two environments and the broad and narrow part of the trapezoid (Supplemental Figure 2AB). Likewise, we contrasted average walking speeds during the replacement phase between the environments and trials targeting objects from the two trapezoid parts (Supplemental Figure 2CD).

Further, we assessed whether the distance from a trial's start position was related to the accuracy of object position memory in a consistent way across subjects. For each subject, we

bioRxiv preprint doi: https://doi.org/10.1101/391201; this version posted August 14, 2018. The copyright holder for this preprint (which was not certified by peer review) is the author/funder, who has granted bioRxiv a license to display the preprint in perpetuity. It is made available under aCC-BY-NC-ND 4.0 International license.

calculated the Spearman correlation coefficient between the distances from start to true object positions and positional memory as defined by the Euclidean distances between true and remembered object positions. The resulting coefficients were tested against 0 for all trials in the two environments separately (Supplemental Figure 2E) or for trials probing objects in the narrow and broad part of the trapezoid, respectively (Supplemental Figure 2F).

In a next step, we assessed rotations participants made during the replacement phase of the trial. To this end, we centered the rotation of the body as measured by the orientation of the motion platform's ring construction and the orientation of the participant's head as tracked by the HMD on the direction from start to response position. We averaged orientation values for trials within square and trapezoid or broad and narrow part of the trapezoid, respectively, and tested for clustering around 0 using V-tests and differences of averaged orientation values between conditions using Watson-Williams tests (Berens, 2009) (Supplemental Figure 3, top row). Additionally, we quantified the circular variance of centered orientation values and contrasted it across conditions (Supplemental Figure 3, bottom row). None of these measures suggested influences of navigation behavior per se on the key conclusions of the paper.

Distance estimation tasks

After completing the time estimation task following the second object position memory task in the second environment, participants estimated distances between pairs of object positions in two modalities: on a computer screen and by walking the actual distances in VR.

Virtual reality

Participants were placed in the same circular virtual arena as during the familiarization session. Each trial began with an arrow pointing to the middle of the arena, with the arrow appearing at a random location on the arena floor. After participants positioned themselves on the base of the arrow, images of two objects were presented in front of them for 3 seconds (Figure 3A). Participants were instructed to walk the distance they remembered the objects to be apart based on the object position memory task while following the direction indicated by the arrow. When participants terminated a trial via button press, a checkmark was presented to indicate the successful registration of the response and the next trial began. Due to time constraints this task was restricted to distances between objects within a triplet, resulting in 12 trials making up a block. Trial order within blocks was randomized with the constraint that trials with objects from the two environments alternated. Participants completed two blocks with a short break in between.

Since only distances within a triplet of positions were tested in this task, participants' averaged estimates for the long and short distances were compared using a bootstrap-based paired t-test as an indicator of successful task performance (Supplemental Figure 4A). To test whether distance estimates for the same distances differed between narrow and broad part

bioRxiv preprint doi: https://doi.org/10.1101/391201; this version posted August 14, 2018. The copyright holder for this preprint (which was not certified by peer review) is the author/funder, who has granted bioRxiv a license to display the preprint in perpetuity. It is made available under aCC-BY-NC-ND 4.0 International license.

of the trapezoid, we took advantage of the fact that true distances were matched across position triplets and thereby arena parts. Response distances within a triplet were averaged and expressed as the log ratio of mean distances in narrow over broad part for statistical comparisons using a bootstrap-based t-test against 0 (Figure 3B). As for the memory ratio, we created a surrogate distribution to compare the distance ratio observed in the trapezoid to the square by shuffling across participants which half of the square was to serve as the numerator and denominator for the distance ratio in each of 10000 permutations. The log distance ratio observed in the trapezoid was more extreme than the 2.5th and 97.5th percentiles (two-tailed test) of this surrogate distribution (Supplemental Figure 4D). The shape of the surrogate distribution did not differ from normality (Kolmogorov-Smirnov test, D=0.01, p=0.287).

Computer monitor

Afterwards, participants were instructed to estimate distances between object pairs on a desktop computer setup. Images of objects on a white background, as well as an adjustable horizontal bar with the labels 'close together' on the left and 'far apart' on the right were presented on a computer screen (Figure 3C). Again, participants were instructed to estimate how far objects were apart during the object location memory task. Here, they indicated their response by adjusting the horizontal bar with a computer mouse, after which a grey screen was shown for 500 milliseconds. All possible combinations of distances were probed, i.e. also comparisons across triplets, yielding subjective distances between all pairs of object positions in an environment. Each of the 15 combinations of object pairs per environment was probed twice, resulting in a total of 60 trials. Trial order was randomized with the constraint that each possible pair of objects was sampled before any object combination was sampled for the second time. Each object was shown once on the left and once on the right side of the screen in the two trials sampling a given object pair. This distance estimation task as well as the time estimation task was presented using the Psychophysics Toolbox (Brainard, 1997) for Matlab (Release 2016a, The MathWorks, Inc.). General performance in this task was assessed by calculating Spearman correlations between the estimated distances and the respective true distances (Supplemental Figure 4B). Further, the remembered distance ratio was calculated and tested in the same way as described above. The surrogate distribution obtained for comparison to the square did not differ from normality (Kolmogorov-Smirnov test, D=0.01, p=0.186).

Reconstructing remembered positions

To reconstruct remembered object positions in the trapezoid from distance estimates, multidimensional scaling (MDS) was applied to the distance estimates obtained in the desktop version of the task as only here distances between all pairs of positions were estimated. Estimated distances were normalized to a range from 0 to 1 and averaged across the two repetitions of each object pair and subjected to MDS to recover coordinates reflecting this distance structure using metric stress as the cost function and a random initial

bioRxiv preprint doi: https://doi.org/10.1101/391201; this version posted August 14, 2018. The copyright holder for this preprint (which was not certified by peer review) is the author/funder, who has granted bioRxiv a license to display the preprint in perpetuity. It is made available under aCC-BY-NC-ND 4.0 International license.

configuration of points. Our approach assumes that two dimensions underlie the object location memory formed during the navigation task. To assess whether this assumption holds, we compared the model deviance of general linear models predicting the distances between true positions from the positions recovered from MDS for different numbers of dimensions. As expected, unexplained variance was substantially decreased when using two instead of one dimension, but no clear improvement resulted from a larger number of dimensions (Supplemental Figure 5).

To match the coordinates resulting from MDS to the original positions in the virtual environment we used Procrustes analysis allowing translation, scaling, reflection and rotation. The goodness of fit, the Procrustes distance, was quantified by the normalized sum of squared errors between reconstructed and true coordinates and was compared to Procrustes distances resulting from Procrustes analyses of the MDS coordinates and sets of coordinates in which the assignment of object identity to position was shuffled, yielding a surrogate distribution from all 720 possible permutations. Specifically, we tested on the group level whether the fits between reconstructed coordinates and true coordinates were better than the fits constituting the 5th percentile (reflecting the threshold for statistical significance at an alpha-level of 0.05) of each participant's surrogate distribution (Figure 4BC). The reconstructed coordinates are visualized as heatmaps in Supplemental Figure 5B following the same procedure as described above.

To test whether the reconstructed positions indeed reflected participants' memory in the object position memory task, we re-calculated the memory scores as described above but with the coordinates resulting from the Procrustes analysis instead of the true object positions as goal positions (Figure 4D). To rule out that objects whose positions were reconstructed to be remembered outside of the environment were driving the effect, we excluded all affected trials from the memory score calculation in an additional control analysis. To describe the overlap between positions reconstructed from distance estimates and performance in the object position memory task, we calculated error vectors based on the true object positions and quantified the match between average error vectors of response and reconstructed positions by correlating their lengths using Pearson correlation (Figure 4E). We further probed these error vectors' similarity in orientation by averaging the angular differences between vectors from the correct to the respective response and reconstructed positions for each participant and testing the resulting circular means for a clustering around 0 using a V-test (Figure 4F).

Time estimation task

Here, we asked participants to perform a secondary task during the navigation period in each arena. In the sky above the arena a ring was presented, which changed color four times during the object position memory task per environment. The ring remained in a given color for an interval between 2 and 6 minutes and participants indicated color changes via button

bioRxiv preprint doi: https://doi.org/10.1101/391201; this version posted August 14, 2018. The copyright holder for this preprint (which was not certified by peer review) is the author/funder, who has granted bioRxiv a license to display the preprint in perpetuity. It is made available under aCC-BY-NC-ND 4.0 International license.

presses and were instructed to remember the order of colors and the duration for which each color was presented. While different colors were presented in the two environments, the intervals between color changes were constant across environments allowing for a comparison of temporal memory between square and trapezoid.

After completing the object position memory task in the first environment, participants were placed in front of a computer screen to estimate the time between color changes before continuing the object position memory task. On a white screen, two pairs of consecutive colors were shown and participants indicated the time interval they remembered to separate the two color changes in minutes and seconds, e.g. how much time passed between the ring changing color from blue to yellow and changing from yellow to green. Participants were cued to estimate the time between all six possible combinations of color changes per environment. To ensure full understanding of this task, participants estimated intervals between color changes occurring at random times between every 30 and 120 seconds during the familiarization phase prior to the object position memory task. Overall performance in this task was quantified using Spearman correlations between the correct and estimated time intervals before specifically comparing average estimation errors, absolute estimation errors and the standard deviation of estimation errors across environments (Supplemental Figure 6).

bioRxiv preprint doi: https://doi.org/10.1101/391201; this version posted August 14, 2018. The copyright holder for this preprint (which was not certified by peer review) is the author/funder, who has granted bioRxiv a license to display the preprint in perpetuity. It is made available under aCC-BY-NC-ND 4.0 International license.

Supplemental Figures

Supplemental Figure 1

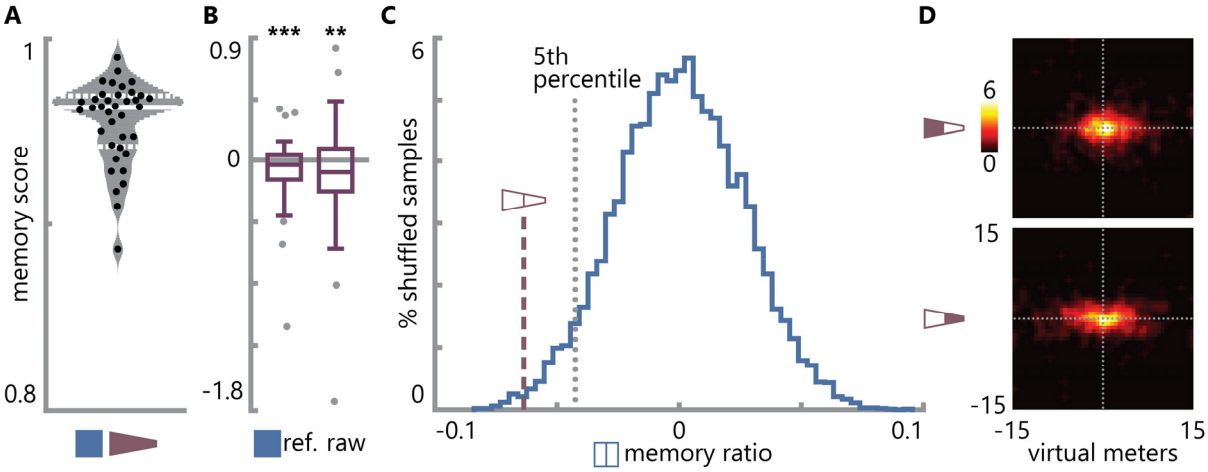

Supplemental Figure 1. Positional memory. A. Distribution of average memory scores across participants. Grey area indicates normal kernel density estimate, solid white line shows median and dashed white lines show upper and lower quartile of distribution. Black circles show memory scores of individual participants. **B.** Log memory ratio for the two parts of the trapezoid for performance referenced to square behavior (left) and for raw error scores (right). Lower values indicate lower performance in the narrow part of the trapezoid and log memory ratios are consistently below zero (referenced to square: $t(30)=-2.52$, $p=9.999\times10^{-5}$; raw error ratio: $t(32)=-1.89$, $p=0.006$). Data points more than 1.5 times the interquartile range above or below the upper or lower quartile were excluded as outliers (grey dots), but comparable results are obtained without outlier exclusion (referenced to square: $t(36)=-1.85$, $p=0.005$; raw error ratio: $t(36)=-1.44$, $p=0.032$). Boxplots represent median as well as upper and lower quartile of distribution, whiskers show most extreme value within 1.5 times the interquartile range from the upper and lower quartile respectively. **C.** The log memory ratio observed between the trapezoid parts (dashed line represents mean of ratio scores shown in Fig. 2E) was significantly lower than the critical value (5th percentile, dotted line) of a shuffle distribution (blue) obtained from computing the log memory ratio between the square halves across 10000 iterations. **D.** Heatmaps showing response locations for all trials across all participants for objects in the broad (top) and narrow (bottom) part of the trapezoid. Dotted lines show correct location in x- and y-dimension with their intersection representing the true position. ** $p<0.01$, *** $p<0.001$

bioRxiv preprint doi: https://doi.org/10.1101/391201; this version posted August 14, 2018. The copyright holder for this preprint (which was not certified by peer review) is the author/funder, who has granted bioRxiv a license to display the preprint in perpetuity. It is made available under aCC-BY-NC-ND 4.0 International license.

Supplemental Figure 2

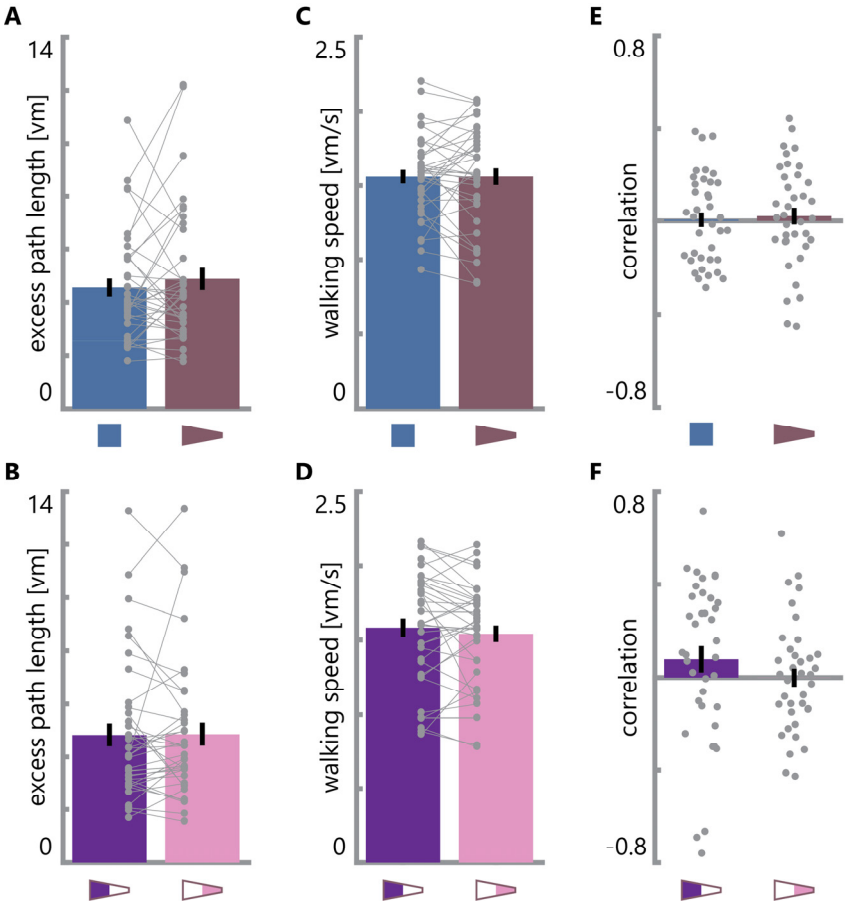

Supplemental Figure 2. Navigational variables do not differ between environments. A,B. The excess path length of the trajectory from start to response position did not differ between square and trapezoid or the two parts of the trapezoid. **C,D.** Walking speed did not differ between square and trapezoid or the two parts of the trapezoid. **E,F.** Spearman correlation coefficients between the Euclidean distance from the start to the correct object positions and replacement error do not differ from 0 across subjects in the square or trapezoid or for objects located in the broad and narrow part of the trapezoid separately. Bars show mean±SEM and grey circles indicate individual subject data with lines connecting data points from the same participant.

bioRxiv preprint doi: https://doi.org/10.1101/391201; this version posted August 14, 2018. The copyright holder for this preprint (which was not certified by peer review) is the author/funder, who has granted bioRxiv a license to display the preprint in perpetuity. It is made available under aCC-BY-NC-ND 4.0 International license.

Supplemental Figure 3

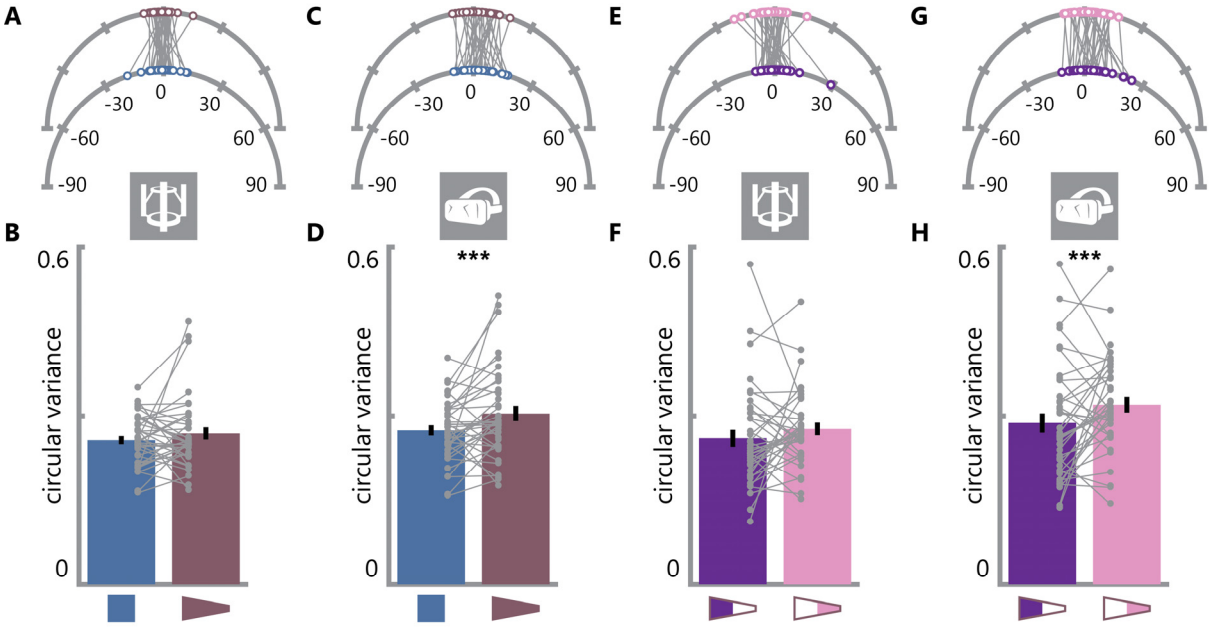

Supplemental Figure 3. Head and body orientation during navigation. A. Circular means of body rotations centered on each trial's direction from start to response position. Means are significantly clustered around 0 for both square and trapezoid and do not differ significantly. **B.** Circular variance of body rotations over trials averaged for each participant does not differ between square and trapezoid. **C.** Circular means of head rotations centered on each trial's direction from start to response position. Means are significantly clustered around 0 for both square and trapezoid and do not differ significantly. **D.** Circular variance of head rotations over trials averaged for each participant is larger in the trapezoid than in the square. **E.** Circular means of body rotations centered on each trial's direction from start to response position. Means are significantly clustered around 0 for trials with target object positions in the broad and narrow part of the trapezoid, respectively, and do not differ significantly. **F.** Circular variance of body rotations over trials averaged for each participant does not differ between navigation periods for target objects located in the broad or narrow portion of the trapezoid. **G.** Circular means of head rotations centered on each trial's direction from start to response position. Means are significantly clustered around 0 for true positions in the broad and narrow part of the trapezoid and do not differ significantly. **H.** Circular variance of head rotations over trials averaged for each participant is smaller when cued object position is in the broad compared to the narrow portion of the trapezoid. *** $p<0.001$

bioRxiv preprint doi: https://doi.org/10.1101/391201; this version posted August 14, 2018. The copyright holder for this preprint (which was not certified by peer review) is the author/funder, who has granted bioRxiv a license to display the preprint in perpetuity. It is made available under aCC-BY-NC-ND 4.0 International license.

Supplemental Figure 4

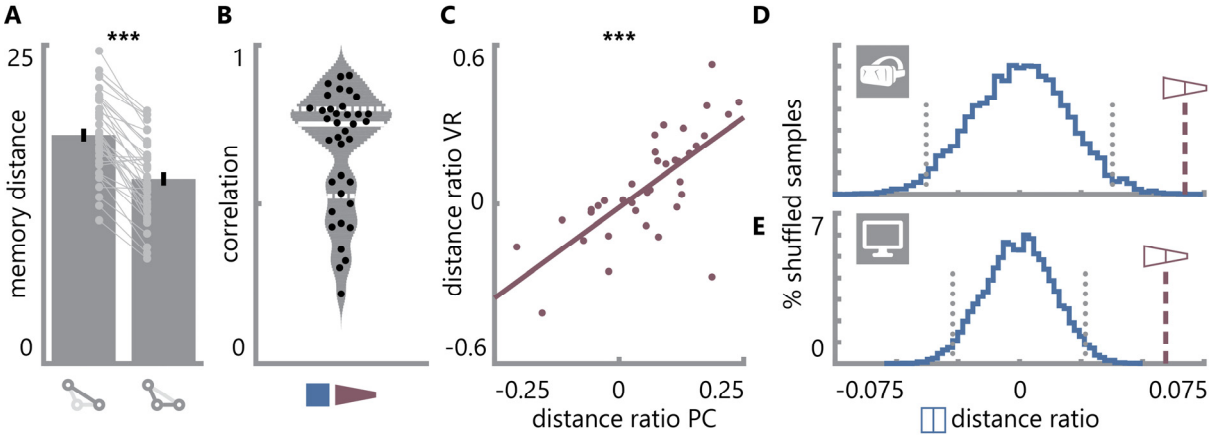

Supplemental Figure 4. Distance estimates. A. Long distances (i.e. the base of the isosceles triangle formed by a triplet of positions) were estimated to be longer than the shorter distances (i.e. the legs of the isosceles triangle). Only within-triplet distances were estimated in VR. Bars show mean±SEM and grey circles indicate individual subject data with lines connecting data points from the same participant. **B.** Grey area indicates distribution of Spearman correlation (mean±SD r=0.69±0.19) coefficients between correct and estimated distances based on normal kernel density estimate. Solid white line shows median and dashed white lines show upper and lower quartile. Black circles show correlation coefficients of individual participants. **C.** Significant Spearman correlation of log distance ratio comparing the two parts of the trapezoid obtained from distance estimates on the desktop and in VR. Circles denote individual participant data. **D,E.** The log distance ratio observed between the trapezoid parts (dashed line) was more extreme than the critical values (dotted line) of the shuffle distribution (blue) obtained from computing the log distance ratio between the square halves across 10000 iterations for the distance estimates in VR (**D**) and on the PC (**E**).

bioRxiv preprint doi: https://doi.org/10.1101/391201; this version posted August 14, 2018. The copyright holder for this preprint (which was not certified by peer review) is the author/funder, who has granted bioRxiv a license to display the preprint in perpetuity. It is made available under aCC-BY-NC-ND 4.0 International license.

Supplemental Figure 5

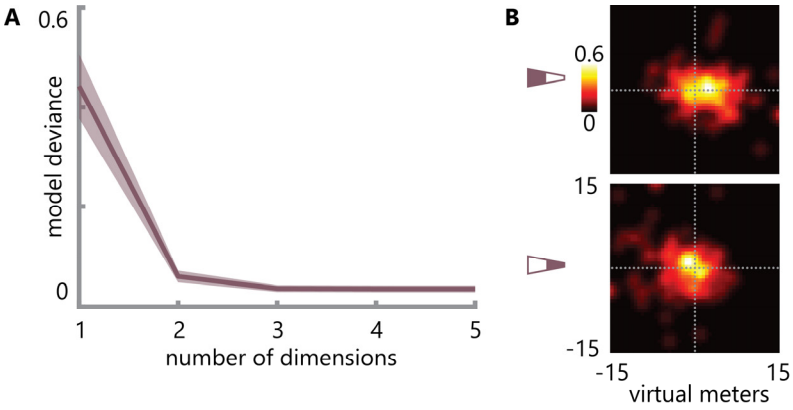

Supplemental Figure 5. Two dimensions underlie distance estimates. A. Model deviance of GLMs using pairwise Euclidean distances of coordinates obtained from MDS to predict estimated distances for different numbers of dimensions (solid line shows mean model deviance across participants, shaded area indicates SEM). In line with our a priori assumption that two dimensions underlie the distance estimates, model deviance sharply drops when using two rather than one dimension and there is no substantial benefit from including three or more dimensions. **B.** Heatmaps showing positions reconstructed using multi-dimensional scaling and Procrustes transform for objects in the broad (top) and narrow (bottom) part of the trapezoid. Dotted lines show correct position in x- and y-dimension with their intersection representing the true position.

bioRxiv preprint doi: https://doi.org/10.1101/391201; this version posted August 14, 2018. The copyright holder for this preprint (which was not certified by peer review) is the author/funder, who has granted bioRxiv a license to display the preprint in perpetuity. It is made available under aCC-BY-NC-ND 4.0 International license.

Supplemental Figure 6

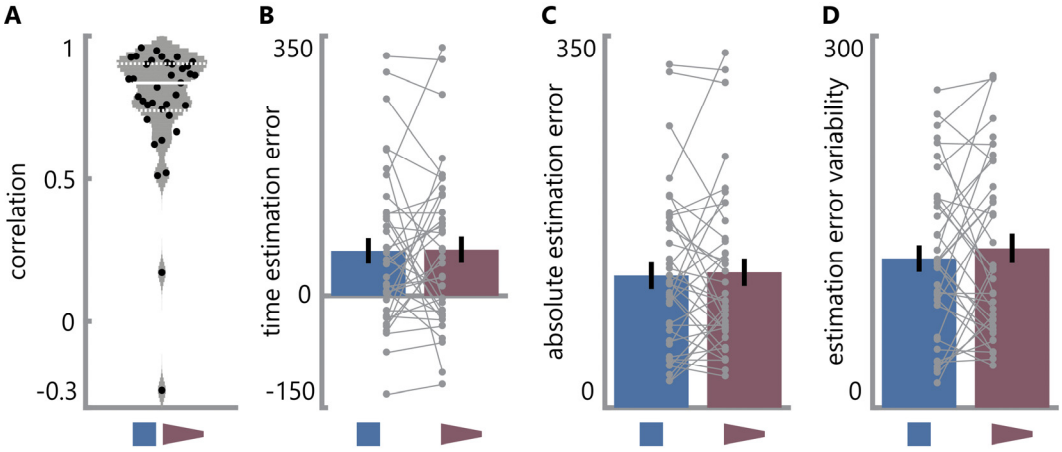

Supplemental Figure 6. Time estimates do not differ between environments. A. Grey area indicates distribution of Spearman correlation coefficients (mean±SD r=0.77±0.23) between true and estimated times based on normal kernel density estimate. Solid white line shows median and dashed white lines show upper and lower quartile. Black circles show correlation coefficients of individual participants. **B.** Averaged time estimation errors did not differ between the two environments. **C.** Averaged absolute time estimation errors did not differ between the two environments. **D.** The variability of time estimates as measured by their standard deviation did not differ between environments. Bars show mean±SEM and grey circles indicate individual subject data with lines connecting data points from the same participant.

bioRxiv preprint doi: https://doi.org/10.1101/391201; this version posted August 14, 2018. The copyright holder for this preprint (which was not certified by peer review) is the author/funder, who has granted bioRxiv a license to display the preprint in perpetuity. It is made available under aCC-BY-NC-ND 4.0 International license.

Acknowledgments

We thank Jackeline Neves Pereira for pilot work leading up to the final experimental design. CFD's research is supported by the Max Planck Society; the European Research Council (ERC-CoG GEOCOG 724836); the Kavli Foundation, the Centre of Excellence scheme of the Research Council of Norway – Centre for Neural Computation, The Egil and Pauline Braathen and Fred Kavli Centre for Cortical Microcircuits, the National Infrastructure scheme of the Research Council of Norway – NORBRAIN; and the Netherlands Organisation for Scientific Research (NWO-Vidi 452-12-009; NWO-Gravitation 024-001-006; NWO-MaGW 406-14-114; NWO-MaGW 406-15-291). The funders had no role in study design, data collection and analysis, decision to publish or preparation of the manuscript.

Author contributions

J.B., C.B. and C.D. conceived the experiment. J.B., T.R., M.N. and C.D. designed the experiment. T.R. collected the data. J.B. analyzed the data and wrote the manuscript, with input from C.B. and C.D. All authors discussed the results and contributed to the final manuscript.

Competing Financial Interests Statement

The authors declare no competing financial interests.

bioRxiv preprint doi: https://doi.org/10.1101/391201; this version posted August 14, 2018. The copyright holder for this preprint (which was not certified by peer review) is the author/funder, who has granted bioRxiv a license to display the preprint in perpetuity. It is made available under aCC-BY-NC-ND 4.0 International license.

References

Aronov, D., Nevers, R., and Tank, D.W. (2017). Mapping of a non-spatial dimension by the hippocampal–entorhinal circuit. Nature *543*, 719–722.

Banino, A., Barry, C., Uria, B., Blundell, C., Lillicrap, T., Mirowski, P., Pritzel, A., Chadwick, M.J., Degris, T., Modayil, J., et al. (2018). Vector-based navigation using grid-like representations in artificial agents. Nature *557*, 429–433.

Barry, C., Hayman, R., Burgess, N., and Jeffery, K.J. (2007). Experience-dependent rescaling of entorhinal grids. Nat Neurosci *10*, 682–684.

Bellmund, J.L.S., Deuker, L., Navarro Schröder, T., and Doeller, C.F. (2016). Grid-cell representations in mental simulation. ELife *5*, e17089.

Berens, P. (2009). CircStat: A MATLAB Toolbox for Circular Statistics. Journal of Statistical Software *31*.

Boto, E., Holmes, N., Leggett, J., Roberts, G., Shah, V., Meyer, S.S., Muñoz, L.D., Mullinger, K.J., Tierney, T.M., Bestmann, S., et al. (2018). Moving magnetoencephalography towards real-world applications with a wearable system. Nature *555*, 657–661.

Brainard, D.H. (1997). The Psychophysics Toolbox. Spatial Vision *10*, 433–436.

Brun, V.H., Solstad, T., Kjelstrup, K.B., Fyhn, M., Witter, M.P., Moser, E.I., and Moser, M.-B. (2008). Progressive increase in grid scale from dorsal to ventral medial entorhinal cortex. Hippocampus *18*, 1200–1212.

Brunec, I.K., Javadi, A.-H., Zisch, F.E.L., and Spiers, H.J. (2017). Contracted time and expanded space: The impact of circumnavigation on judgements of space and time. Cognition *166*, 425–432.

Buckner, R.L. (2010). The role of the hippocampus in prediction and imagination. Annual Review of Psychology *61*, 27–48.

Burak, Y., and Fiete, I.R. (2009). Accurate Path Integration in Continuous Attractor Network Models of Grid Cells. PLOS Computational Biology *5*, e1000291.

Bush, D., Barry, C., Manson, D., and Burgess, N. (2015). Using Grid Cells for Navigation. Neuron *87*, 507–520.

Byrne, P., Becker, S., and Burgess, N. (2007). Remembering the past and imagining the future: a neural model of spatial memory and imagery. Psychological Review *114*, 340–375.

Cakmak, T., and Hager, H. (2014). Cyberith virtualizer: a locomotion device for virtual reality. In ACM SIGGRAPH 2014 Emerging Technologies, (ACM), p. 6.

Campbell, M.G., Ocko, S.A., Mallory, C.S., Low, I.I.C., Ganguli, S., and Giocomo, L.M. (2018). Principles governing the integration of landmark and self-motion cues in entorhinal cortical codes for navigation. Nature Neuroscience *21*, 1096–1106.

Carpenter, F., and Barry, C. (2016). Distorted Grids as a Spatial Label and Metric. Trends in Cognitive Sciences *20*, 164–167.

Chen, X., He, Q., Kelly, J.W., Fiete, I.R., and McNamara, T.P. (2015). Bias in Human Path Integration Is Predicted by Properties of Grid Cells. Current Biology *25*, 1771–1776.

Constantinescu, A.O., O'Reilly, J.X., and Behrens, T.E.J. (2016). Organizing conceptual knowledge in humans with a gridlike code. Science *352*, 1464–1468.

bioRxiv preprint doi: https://doi.org/10.1101/391201; this version posted August 14, 2018. The copyright holder for this preprint (which was not certified by peer review) is the author/funder, who has granted bioRxiv a license to display the preprint in perpetuity. It is made available under aCC-BY-NC-ND 4.0 International license.

Doeller, C.F., Barry, C., and Burgess, N. (2010). Evidence for grid cells in a human memory network. Nature *463*, 657–661.

Epstein, R.A., Patai, E.Z., Julian, J.B., and Spiers, H.J. (2017). The cognitive map in humans: spatial navigation and beyond. Nature Neuroscience *20*, 1504.

Erdem, U.M., and Hasselmo, M. (2012). A goal-directed spatial navigation model using forward trajectory planning based on grid cells: Forward linear look-ahead trajectory model. European Journal of Neuroscience *35*, 916–931.

Fiete, I.R., Burak, Y., and Brookings, T. (2008). What Grid Cells Convey about Rat Location. J. Neurosci. *28*, 6858–6871.

Fyhn, M., Hafting, T., Treves, A., Moser, M.-B., and Moser, E.I. (2007). Hippocampal remapping and grid realignment in entorhinal cortex. Nature *446*, 190–194.

Gardner, R.J., Lu, L., Wernle, T., Moser, M.-B., and Moser, E.I. (2017). Correlation structure of grid cells is preserved during sleep. BioRxiv 198499.

Gil, M., Ancau, M., Schlesiger, M.I., Neitz, A., Allen, K., De Marco, R.J., and Monyer, H. (2018). Impaired path integration in mice with disrupted grid cell firing. Nature Neuroscience *21*, 81–91.

Hafting, T., Fyhn, M., Molden, S., Moser, M.-B., and Moser, E.I. (2005). Microstructure of a spatial map in the entorhinal cortex. Nature *436*, 801–806.

Hartley, T., Trinkler, I., and Burgess, N. (2004). Geometric determinants of human spatial memory. Cognition *94*, 39–75.

Hasselmo, M.E. (2011). How We Remember: Brain Mechanisms of Episodic Memory (Cambridge, MA, US: The MIT Press).

Herz, A.V., Mathis, A., and Stemmler, M. (2017). Periodic population codes: From a single circular variable to higher dimensions, multiple nested scales, and conceptual spaces. Current Opinion in Neurobiology *46*, 99–108.

Horner, A.J., Bisby, J.A., Zotow, E., Bush, D., and Burgess, N. (2016). Grid-like processing of imagined navigation. Current Biology *26*, 842–847.

Jacobs, J., Weidemann, C.T., Miller, J.F., Solway, A., Burke, J.F., Wei, X.-X., Suthana, N., Sperling, M.R., Sharan, A.D., Fried, I., et al. (2013). Direct recordings of grid-like neuronal activity in human spatial navigation. Nature Neuroscience *16*, 1188–1190.

Jacobs, J., Miller, J., Lee, S.A., Coffey, T., Watrous, A.J., Sperling, M.R., Sharan, A., Worrell, G., Berry, B., Lega, B., et al. (2016). Direct Electrical Stimulation of the Human Entorhinal Region and Hippocampus Impairs Memory. Neuron *92*, 983–990.

Jafarpour, A., and Spiers, H. (2017). Familiarity expands space and contracts time. Hippocampus *27*, 12–16.

Julian, J.B., Keinath, A.T., Frazzetta, G., and Epstein, R.A. (2018). Human entorhinal cortex represents visual space using a boundary-anchored grid. Nature Neuroscience.

Kelly, J.W., McNamara, T.P., Bodenheimer, B., Carr, T.H., and Rieser, J.J. (2008). The shape of human navigation: How environmental geometry is used in maintenance of spatial orientation. Cognition *109*, 281–286.

Killian, N.J., Jutras, M.J., and Buffalo, E. a. (2012). A map of visual space in the primate entorhinal cortex. Nature *491*, 761–764.

bioRxiv preprint doi: https://doi.org/10.1101/391201; this version posted August 14, 2018. The copyright holder for this preprint (which was not certified by peer review) is the author/funder, who has granted bioRxiv a license to display the preprint in perpetuity. It is made available under aCC-BY-NC-ND 4.0 International license.

Kraus, B.J., Brandon, M.P., Robinson, R.J., Connerney, M.A., Hasselmo, M.E., and Eichenbaum, H. (2015). During Running in Place, Grid Cells Integrate Elapsed Time and Distance Run. Neuron *88*, 578–589.

Krupic, J., Bauza, M., Burton, S., Barry, C., and O'Keefe, J. (2015). Grid cell symmetry is shaped by environmental geometry. Nature *518*, 232–235.

Krupic, J., Bauza, M., Burton, S., and O'Keefe, J. (2018). Local transformations of the hippocampal cognitive map. Science *359*, 1143–1146.

Kubie, J.L., and Fenton, A.A. (2012). Linear Look-Ahead in Conjunctive Cells: An Entorhinal Mechanism for Vector-Based Navigation. Front. Neural Circuits *6*.

Kunz, L., Navarro Schröder, T., Lee, H., Montag, C., Lachmann, B., Sariyska, R., Reuter, M., Stirnberg, R., Stöcker, T., Messing-Floeter, P.C., et al. (2015). Reduced grid-cell–like representations in adults at genetic risk for Alzheimer's disease. Science *350*, 430–433.

Mathis, A., Herz, A.V.M., and Stemmler, M. (2012). Optimal Population Codes for Space: Grid Cells Outperform Place Cells. Neural Computation *24*, 2280–2317.

McNaughton, B.L., Battaglia, F.P., Jensen, O., Moser, E.I., and Moser, M.-B. (2006). Path integration and the neural basis of the "cognitive map." Nature Reviews Neuroscience *7*, 663–678.

Moser, E.I., Moser, M.-B., and McNaughton, B.L. (2017). Spatial representation in the hippocampal formation: a history. Nature Neuroscience *20*, 1448–1464.

Nadasdy, Z., Nguyen, T.P., Török, Á., Shen, J.Y., Briggs, D.E., Modur, P.N., and Buchanan, R.J. (2017). Context-dependent spatially periodic activity in the human entorhinal cortex. Proceedings of the National Academy of Sciences *114*, E3516–E3525.

Nau, M., Navarro Schröder, T., Bellmund, J.L.S., and Doeller, C.F. (2018). Hexadirectional coding of visual space in human entorhinal cortex. Nature Neuroscience.

Navarro Schröder, T., Towse, B.W., Burgess, N., Barry, C., and Doeller, C.F. (2017). Optimal decision making using grid cells under spatial uncertainty. BioRxiv 166306.

O'Keefe, J., and Dostrovsky, J. (1971). The hippocampus as a spatial map. Preliminary evidence from unit activity in the freely-moving rat. Brain Research *34*, 171–175.

O'Keefe, J., and Nadel, L. (1978). The Hippocampus as a Cognitive Map (Oxford: Clarendon Press).

Schuck, N.W., Doeller, C.F., Polk, T.A., Lindenberger, U., and Li, S.-C. (2015). Human aging alters the neural computation and representation of space. NeuroImage *117*, 141–150.

Stangl, M., Achtzehn, J., Huber, K., Dietrich, C., Tempelmann, C., and Wolbers, T. (2018). Compromised Grid-Cell-like Representations in Old Age as a Key Mechanism to Explain Age-Related Navigational Deficits. Current Biology *28*, 1108-1115.e6.

Stensola, H., Stensola, T., Solstad, T., Frøland, K., Moser, M.-B., and Moser, E.I. (2012). The entorhinal grid map is discretized. Nature *492*, 72–78.

Stensola, T., Stensola, H., Moser, M.-B., and Moser, E.I. (2015). Shearing-induced asymmetry in entorhinal grid cells. Nature *518*, 207–212.

Sun, C., Kitamura, T., Yamamoto, J., Martin, J., Pignatelli, M., Kitch, L.J., Schnitzer, M.J., and Tonegawa, S. (2015). Distinct speed dependence of entorhinal island and ocean cells, including respective grid cells. PNAS *112*, 9466–9471.

bioRxiv preprint doi: https://doi.org/10.1101/391201; this version posted August 14, 2018. The copyright holder for this preprint (which was not certified by peer review) is the author/funder, who has granted bioRxiv a license to display the preprint in perpetuity. It is made available under aCC-BY-NC-ND 4.0 International license.

Taube, J.S., Valerio, S., and Yoder, R.M. (2013). Is Navigation in Virtual Reality with fMRI Really Navigation? Journal of Cognitive Neuroscience *25*, 1008–1019.

Trettel, S.G., Trimper, J.B., Hwaun, E., Fiete, I.R., and Colgin, L.L. (2017). Grid cell co-activity patterns during sleep reflect spatial overlap of grid fields during active behaviors. BioRxiv 198671.

Yoon, K., Buice, M.A., Barry, C., Hayman, R., Burgess, N., and Fiete, I.R. (2013). Specific evidence of low-dimensional continuous attractor dynamics in grid cells. Nature Neuroscience *16*, 1077–1084.